Engineering and Technology Journal
Journal homepage: https://etj.uotechnology.edu.iq

Investigation of Fe_3O_4 nanoparticles synthesized via co-precipitation coated with chitosan, PEG, and folate for targeted paclitaxel delivery in fibrosarcoma treatment

Adawiya J. Haider [a], Sharafaldin M. Al-Musawi [b], Rusul A. Al-Obaidy [c], Azhar M. Haleem[d], Mohammed S. Al-Hindawi [a]*, Bakr Ahmed Taha [e]

[a] Applied Sciences Dept., University of Technology- Iraq, Alsina'a street, 10066 Baghdad, Iraq.
[b] College of Food Sciences, Al-Qasim Green University, Babylon, Iraq.
[c] Minsitry of Industry and Minerals Industrial Development and Regulatory Directorate, Baghdad-Iraq
[d] Environmental Research Center, University of Technology, Alsina'a street, 10066 Baghdad-Iraq
[e] Photonics Technology Laboratory, Dept., of Electrical, Electronic and Systems Engineering, Faculty of Engineering and Built Environment, Universiti Kebangsaan Malaysia UKM, 43600 Bangi, Malaysia.
*Corresponding author Email: Mohammed.S.AlHindawi@uotechnology.edu.iq

HIGHLIGHTS

- Magnetite (Fe_3O_4) (NPs) were synthesized and optimized to control particle size and morphology.
- Fe_3O_4 where modified to form nanoencapsulated Fe_3O_4@Cs-PEG-PTX-FA particles with sizes ranging from 100 to 130 nm.
- Encapsulation efficiency of 82.4% and drug-loading content of 14.4% were achieved.

Keywords:

Fe_3O_4 NPs
Fibrosarcoma
Chitosan
PTX
Co-precipitation

ABSTRACT

Magnetite (Fe_3O_4) nanoparticles (NPs) were synthesized using a straightforward co-precipitation method from Fe_2+/Fe_3+ salt solutions as starting materials. This method was optimized to control particle size and morphology, resulting in highly magnetic NPs with crystallite sizes ranging from 20 to 70 nm. The synthesis process involved magnetic stirring at 700 rpm at room temperature, yielding approximately 5 mg of Fe_3O_4 powder. Structural characterization via X-ray diffraction (XRD) confirmed the stoichiometric composition and particle dimensions. To enhance functionality, the Fe_3O_4 NPs were coated with chitosan (Cs), polyethylene glycol (PEG), and folic acid (FA), and loaded with the anticancer drug paclitaxel (PTX), forming nanoencapsulated Fe_3O_4@Cs-PEG-PTX-FA particles with sizes ranging from 100 to 130 nm. Magnetic properties were assessed using a vibrating sample magnetometer (VSM), revealing saturation magnetization (Ms) values of 59.6 emu/mg for Fe_3O_4 and 19.9 emu/mg for Fe_3O_4@Cs-PEG-PTX-FA. Encapsulation efficiency of 82.4% and drug-loading content of 14.4% were achieved. These results demonstrate the potential of Fe_3O_4 NPs as multifunctional agents in the biomedical field, particularly for targeted drug delivery systems, where magnetic properties can facilitate precise localization and release of therapeutic agents. In addition to size uniformity, biocompatibility, and responsiveness to external magnetic fields make, these properties make them promising candidates for cancer treatment, particularly in targeting fibrosarcoma cells.

1. Introduction

Magnetic nanoparticles, particularly Fe_3O_4, have been extensively researched and used in the last ten years for biomedical purposes, such as magnetized scaffolds [1], gene transfer [2], cell treatment [3,4], magnetic resonance imaging [5-7], cell labeling [8] and hyperthermia [9]. Also, there are many metal oxides like Znic oxide dopants with magnetic material such as cobalt and multiwall carbon nanotubes (MWCNT) decorated with silver nanoparticles that were used as sensors and demonstrated antibacterial effects [10,11]. Researchers have used a variety of techniques to generate Fe_3O_4 on the nanoscale. The most popular approach for creating aqueous Fe^{2+}/Fe^{3+} salt solutions with a base, either at ambient or elevated temperatures. This procedure is simple and precise performance, achieving a success rate of 96% to 99.9% for the generating of Fe_3O_4 nanoparticles (NPs). This procedure uses an alkaline medium containing ferrous and ferric ions in a 1:2 ratio. It enables the production of both single- and multi-component metal oxides as fine, stoichiometric particles. The process involves a nucleation and growth mechanism, resulting in the formation of Fe_3O_4 nanoparticles [12]. A small size distribution and beneficial dispersibility in aquatic environments are desirable properties for Fe_3O_4 magnetic nanoparticles [13].

http://doi.org/10.30684/etj.2025.155892.1867
Received 15 December 2024; Received in revised form 10 January 2025; Accepted 28 January 2025; Available online 26 February 2025
2412-0758/University of Technology-Iraq, Baghdad, Iraq

However, in order to create spherically shaped nanoparticles, the co-precipitation method is a straightforward synthesis technique that uses cheap substrates [14].

Kang et al. [15], reported the synthesis of Fe_3O_4 nanopowders having 15 nm average diameter and cubic shapes via the ultrasonic-assisted co-precipitation method. Ferrite NPs are the iron oxides in the crystal structure of maghemite or magnetite [16]. These are the most explored magnetic NPs to date. Whenever the size of ferrite particles is minimized to less than 128 nm, they exhibit superparamagnetic behavior. This property prevents self-agglomeration, as the nanoparticles only display magnetic behavior by applying an exterior magnetic field. Using $FeCl_3.6H_2O$ and $FeCl_2.4H_2O$ as primary precursors, according to Islam et al. [17], an ultrasonic technology with a maximum power of 1500W and a frequency of 20 kHz for 75 minutes was used to create Fe_3O_4 NPs. According to the findings, the saturation magnetization of the Fe_3O_4 particles was 80 emu/g, and their size was around 11 nm. Furthermore, Choi et al. [18], employed several nanocarriers, such as polymer micelles, liposomes, dendrimers, silicon dioxide NP, and polydrug conjugates. Tumors can be effectively treated by reducing resistance to treatment and adverse effects. NPs offer a promising solution by integrating therapeutic agents with innovative treatment strategies, enhancing the efficacy and precision of cancer therapies. Sood et al. [19], established carbon-coated Fe_3O_4/Au^+ curcumin Core@Shell stabilized by the co-precipitation method using thiolated sodium alginate for biomedical applications.

A TEM micrograph presented by Al-Kinani et al. [20] achieved an average diameter of 20 ± 2.1 nm for Fe_3O_4 NP. Numerous researchers have used primary commercial precursors to produce Fe_3O_4 NPs chemically. The current work discusses utilizing iron salts as a raw material for the production of Fe_3O_4 NPs. The outcomes of the characterization and optimization of the synthesis are also investigated. Fe_3O_4 NPs' form and characteristics are believed to be influenced by the synthesis parameters. The primary objective of this study is to enhance superparamagnetic Fe_3O_4 nanoparticles (NPs) with uniform particle sizes, making them suitable as nanocarriers for biological applications, particularly in antitumor therapy. This is achieved by coating the NPs with biocompatible chitosan (Cs) to encapsulate the drug and facilitate its release at the target site in response to acidic pH, and polyethylene glycol (PEG) to extend blood circulation time while preserving the chemical structure and therapeutic properties of paclitaxel (PTX). Furthermore, the nanocarriers are functionalized with folic acid (FA) to enable targeted drug delivery, forming Fe_3O_4@CS-PEG-PTX-FA NPs. Furthermore, the impact of techniques on the size and shape of Fe_3O_4 crystallites will be explored.

2. Materials and methods

All chemicals used in this study were purchased from Sigma-Aldrich in St. Louis, MO (USA). Low-molecular-weight chitosan (CS) was obtained from Durect Corporation (AL, USA).

2.1 Synthesis of Fe_3O_4 nanoparticles

An exact synthesis of Fe_3O_4 nanoparticles was crucial for the first stages of this ground-breaking project. A precise amount of 0.6 g of ferrous chloride tetrahydrate ($FeCl_2 \cdot 4H_2O$) and 1.2 g of ferric chloride hexahydrate ($FeCl_3.6H_2O$) were carefully dissolved in 10 mL of deionized water (DDW) in a flask, ensuring accuracy and caution during preparation. After being rapidly stirred at room temperature (25 °C) for 15 minutes, the combination experienced a remarkable transition, forming a homogeneous and highly resonant dark orange solution. The subsequent step required meticulous accuracy: gradually adding 10 M ammonium hydroxide (NH_4OH) to the obtained liquid while stirring it at 800 rpm. The pH remained stable throughout a series of meticulously coordinated processes. The solution underwent notable metamorphosis when the base mixed, changing from a dark orange to a profound obsidian black. The alchemical process involved heating the transforming fluid to 80 degrees Celsius for 45 minutes combined with vortexing at 800 rpm. The genesis of Fe_3O_4 can be summed up in the following elegantly condensed Equation (1), which describes the complex interplay of variables that led to its formation.

$$Fe^{2+}+2Fe^{3+}+8OH^- \rightarrow Fe(OH)_2+2Fe(OH)_3 \rightarrow Fe_3O_4\downarrow+4H_2O \quad (1)$$

In this symphony of chemical ingenuity, the synthesis of Fe_3O_4 nanoparticles stood as a testament to precision, distinguished by each calculated addition and orchestrated transformation, all converging toward the creation of a remarkable nanomaterial with immense potential, as shown in Figure 1.

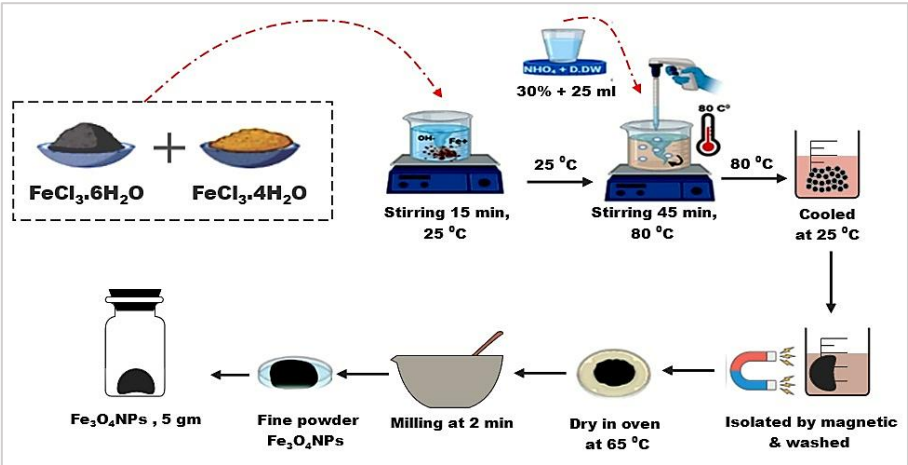

Figure 1: Illustrated steps of the co-precipitation preparation method of Fe_3O_4 NPs in the chemical method to produce 5 mg with Fe_3O_4 NPs as powder

2.2 Formulation of Fe_3O_4@Cs-PTX-PEG-FA nanocarrier

10 mg/mL of chitosan (Cs) and 12 mg/mL of SPION were dissolved in a 1% acetic acid solution. The mixture was treated with ultrasound for 20 minutes to ensure uniformity. Separately, dimethyl sulfoxide (DMSO) was utilized to dissolve 20 mg of paclitaxel (PTX). The obtained solution was then added to 10 mL of the SPION@Cs solution under magnetic stirring at 1000 rpm at room temperature (RT), forming the SPION@Cs-PTX solution.

Next, this solution was slowly and gradually added into 4 mL of a 2 mg/mL TPP solution while stirring at 200 rpm at RT. The nanoparticles formed immediately and were further bonded by stirring at 25 °C for 90 minutes. These nanoparticles were collected by centrifuging at 1500 rpm, followed by using a vacuum oven to dry the nanoparticles at 40 °C for 24 hours [21].

To coat the nanoparticles with PEG, a solution comprising 10% of the volume of total water was prepared and stirred into the SPION@Cs-PTX mixture at 300 rpm for 1 hour at RT. Finally, a 5 mg/mL folic acid (FA) solution was added gradually to the mixture while stirring at 200 rpm for 10 minutes. The encapsulated nanoparticles (SPION@Cs-PTX-PEG-FA) were then spun at 1500 rpm and frozen at -30 °C for 20 hours. Figure 2 illustrates the preparation of Fe3O4@Cs-PTX-PEG-FA nanoparticles. Standard formula Equation (2) and (3), were applied to determine the encapsulation efficacy and medication loading content [22- 24].

$$\text{Encapsulation efficiency (\%)} = \frac{\text{Total amount of drug - Free drug}}{\text{The initial amount of drug}} \times 100 \quad (2)$$

$$\text{Drug loading content (\%)} = \frac{\text{Total amount of drug - Free drug}}{\text{The total amount of nanoparticles}} \times 100 \quad (3)$$

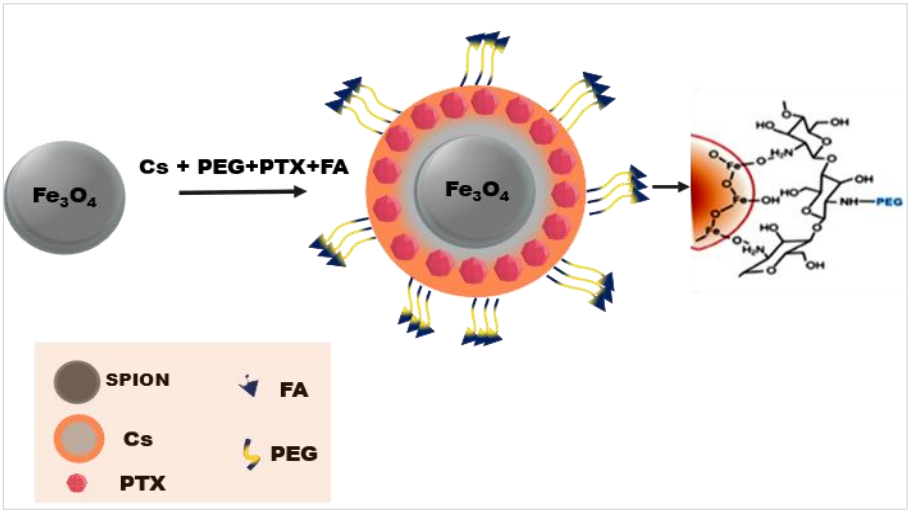

Figure 2: Sceth illustration of the preparation of Fe_3O_4@Cs-PTX-PEG-FA nanoparticles

2.3 Comprehensive characterization of materials

The products' crystal structure was studied employing X-ray diffraction (XRD), Shimadzu XRD-6000 (Japan), model (Miniflex IL, USA). Patterns with Cu Kα radiation (λ = 1,54051 Å) at a voltage of 30 kV, current of 25 mA, and scan interval of 1°/min, recorded in the region of 2θ range of 10 ℃ to 65 ℃.

Scanning electron microscope-energy dispersive X-ray spectrometry (SEM-EDS), a thermofisher firm, was used to evaluate the morphology of Fe_3O_4 materials. The size of the 120 nanoparticles was measured employing a JEM-2000 EXII transmission electron microscope (TEM) from JEOL in Tokyo, Japan. A drop of diluted PTX nanoformulation solution was applied to a 200-mesh formvar carbon-coated copper grid (TABB Laboratories Equipment). Vibrating sample magnetometers (VSM) were used to test the magnetic characteristics of Fe_3O_4 before and after coating. (Lakeshore 7404, USA) at RT.

3. Results and discussion

3.1 Impact of ultra-sonication on nanoparticle characteristics

This novel strategy originates from the idea that a coarse mixture undergoes a transforming process within the ultrasonic field. The expansion of the surrounding atmosphere causes bubbles to form. When these bubbles burst, they release shear forces that effectively break apart large particles into many smaller ones. This method also helps reduce the impact of bubbles, which can impede the growth of nanoparticles. After around 15–20 minutes of using the ultrasonic device, the nanoparticle scale reaches a near-steady state of equilibrium. Notably, this technique uses liquid to control temperature as needed [25]. Figure 3 illustrates this complex interplay of variables.

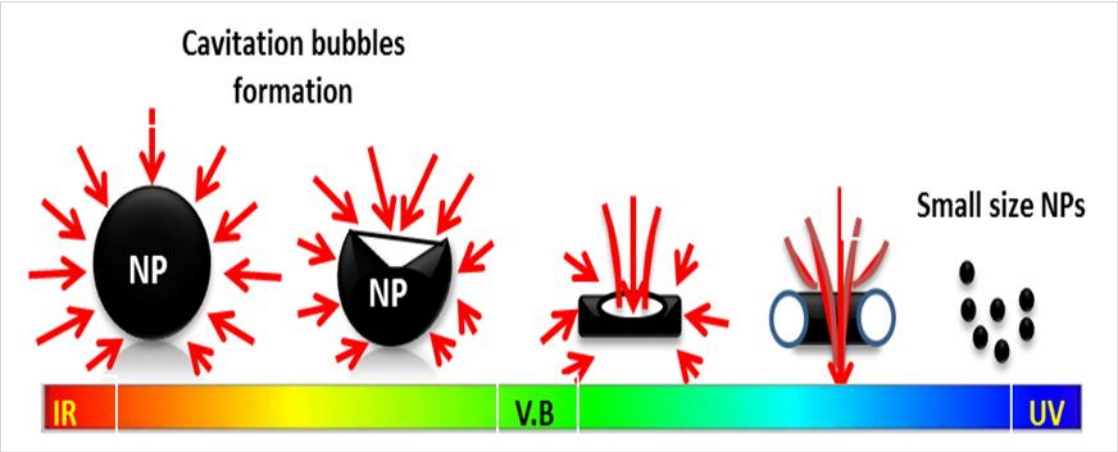

Figure 3: Effect of the ultrasonic device on NPs

3.2 X-ray diffraction insights into uncoated Fe_3O_4 NPs

X-ray diffraction (XRD) played a pivotal role in unraveling the intricate crystal structure of the sample. Figures 4(a) and 4(b) serve as visual testaments, illustrating the crystalline nature of Fe_3O_4 nanoparticles. Remarkably, similar to the findings reported in the referenced study, our materials exhibited diffractions of Fe_3O_4 alongside other iron oxide counterparts, lending credibility to our study [26]. The comprehensive spectrum of peaks encompassing the complete profile of Fe_3O_4 NPs prepared through the co-precipitation method, uncoated (a). Emanating from this data are sharply defined peaks that unveil distinct crystalline regions. Within this tapestry of insights, 10 mountains stood out with maximal peak-to-noise ratios of up to 11.2. We conducted this meticulous analysis under the parameters of ADX-2700 SSC with a power of 40kV and a current of 30 mA.

It is a meticulously set slit configuration of (1 degree) for both θ and 2θ, complemented by a 0.2 mm monochromatic slit, culminated in precise measurements (onTs-Td). The resulting diffraction angles included 18.524°, 30.295°, 35.647°, 37.294°, 43.301°, 53.629°, 57.208°, 62.8°, 71.245°, and 74.291°, each intricately tied to their corresponding indices, namely (111), (220), (311), (222), (400), (422), (511), (440), (620), and (533), thereby unveiling the crystalline facets [24]. The concordance with standard data as per the (JCPDS file 99-0073), adds a layer of robustness to our findings. The discerning eye might note the broadness of these peaks, a characteristic that underscores the nanoparticles' ultrafine constitution and diminutive crystallite dimensions. Remarkably, within this complex tapestry of XRD data, the unmistakable signature of a single cubic phase for Fe_3O_4 nanopowder emerges, enhancing the clarity and significance of our results.

Fe_3O_4 nanoparticles coated with polymers containing the drug PXT (Fe_3O_4@PXT-Cs-PEG-FA) exhibit low-intensity reflection planes in Table 1 and Figure 4(b). Displaying crystalline areas, ID Extended Report (5 Peaks, 2=30.295°, 36.601°, 45.792°, 57.48°, and 67.199°), with indices of (220), (311), (400), (511) and (440), respectively.

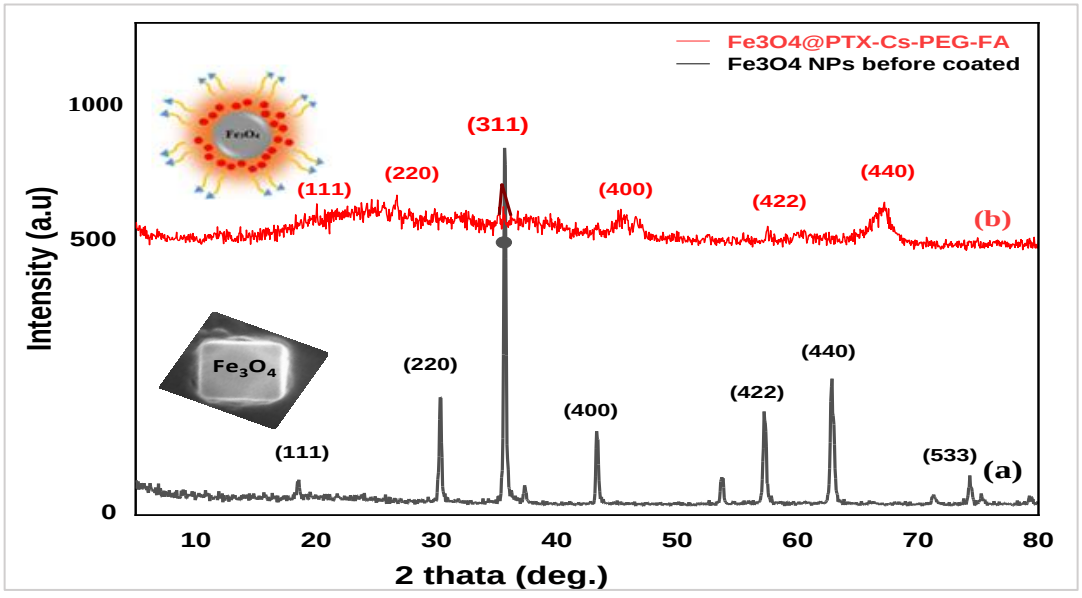

Figure 4: X-ray diffraction of the Fe_3O_4 NP pattern of Fe_3O_4 NPs was prepared using a chemical method before coating (a) and after coating Fe3O4 NPs with polymer (b)

Chaverra et al. [26] claimed that Fe_3O_4 had a higher intensity and longer laser wavelength, an inverted spinel structure, and no additional phase-only magnetites. In an inverse spinel structure, eight Fe^{3+} and eight Fe^{2+} ions alternately occupy tetrahedral and octahedral locations with variable peak intensities. Peak broadening of XRD data can be used with the Scherer Equation [roshan] Equation (4) to determine the sizes of Fe_3O_4 crystallites.

$$D = k^*\lambda / (\beta^*\cos\theta) \quad (4)$$

The wavelength of the XRD beam is represented by λ, while D is the size of crystallite in nanometers (nm). The grain shape constant, k, is typically 0.89 for spherical particles. The term β refers to the full width at half maximum (FWHM) of the diffraction peak, expressed in radians, and θ\thetaθ represents the angle of diffraction. Based on Equation (1), larger particle sizes in Fe_3O_4 samples corresponded to peaks with greater intensity, likely due to the presence of more crystallographic planes, as illustrated in Table 1.

Furthermore, Figure 5 indicates that the crystallite size of nanoparticles tends to increase gradually after polymer coating. This phenomenon can be explained by the kinetic energy gained by the sample, which promotes particle dispersion, reduces Fe_3O_4 molecular weight, and fragments the agglomerated particles into smaller units [27].

Table 1: All peaks of Fe_3O_4@Cs-PEG-PTX-FA fabricated by the reverse micro-emulsion procedure

Peak no.	2θ(deg.)	(hkl)	D(nm)=Kλ/βcosθ	d EXP.	Δ d	Shape
1	30.295	(220)	48.32989654	0.295	0.005	Spinal
2	36.601	(311)	89.24683497	0.245	0.118	Spinal
3	45.792	(400)	114.1015597	0.198	0.0055	Spinal
4	57.48	(511)	182.1249088	0.16	0.169	Spinal
5	67.199	(440)	231.6864984	0.139	0.005	Spinal

According to Figure 5 (a and b), Fe_3O_4 nanoparticles typically have a cubic or spherical shape and are made up of isolated and clustered particles. Clustering of NPs can occur due to a variety of factors, including magnetic interaction between particles [28], the formation of non-uniform cavitation bubbles [29], and an increase in surface free energy due to the reduction in Fe_3O_4 size [30].

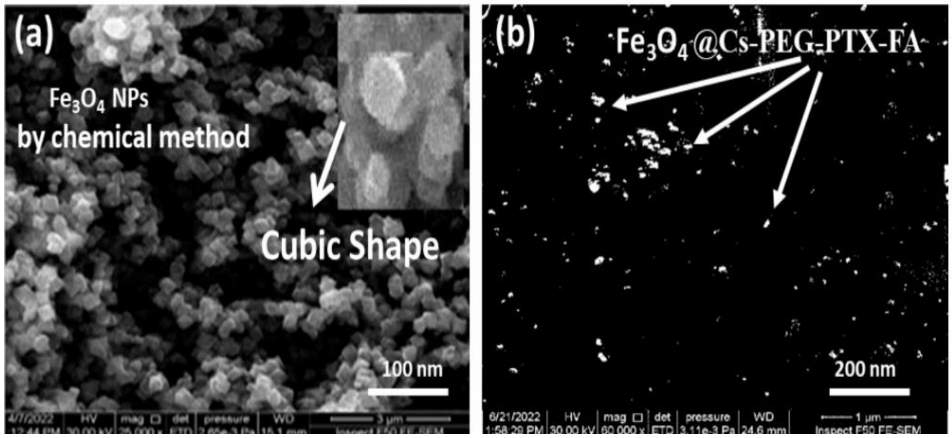

Figure 5: SEM of (a)Fe_3O_4 NP was prepared using a chemical method before Coating, and (b)Fe_3O_4@Cs-PEG-PTX-FA

3.3 Morphological and structural attributes of processed Fe_3O_4

The encapsulation performance and loading content of PTX were 82.4 ± 0.21% and 14.41 ± 0.18%, respectively. Figure 6 shows an EDX spectrum of powder Fe_3O_4 after the chemical method synthesis. The EDX spectra revealed significant Fe and O peaks. The constituents of Fe_3O_4 nanoparticles were prepared using the co-precipitation method, with the associated analysis presented in the table within the figure. These results confirm the purity of the synthesized materials, which are undergoing further investigation.

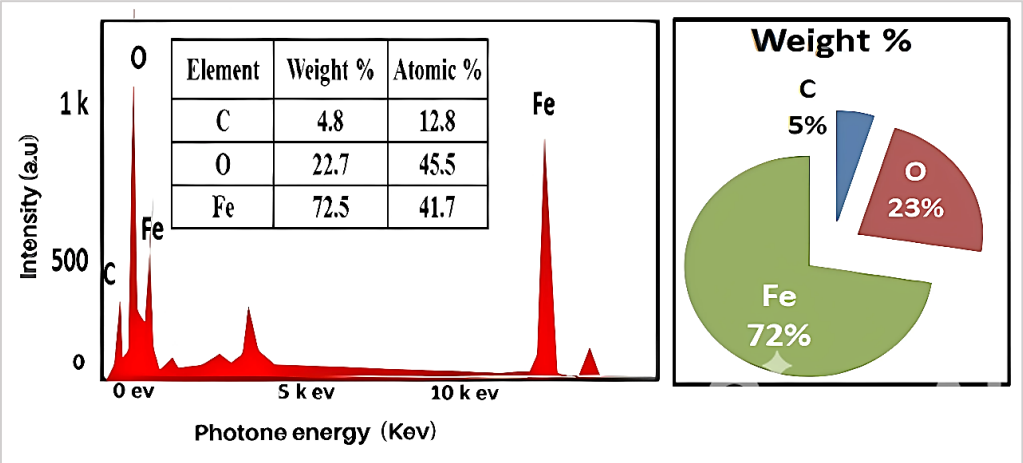

Figure 6: EDX of Fe_3O_4 NP powder with a weight ratio of all elements

3.4 Magnetic characteristics of Fe_3O_4 before and after coating

Figure 7 illustrates the transmission electron microscopy (TEM) images of Fe_3O_4 nanoparticles, providing detailed insights into their size and morphology. The Fe_3O_4 nanoparticles synthesized via the co-precipitation method, using $FeCl_3 \cdot 6H_2O$, $FeCl_2 \cdot 4H_2O$, and ammonium hydroxide as precursors, exhibit a particle size range of 10-40 nm, with an average size below 50 nm as shown in Figure 7(a) [31]. Upon coating with chitosan (Cs), polyethylene glycol (PEG), folic acid (FA), and loading with paclitaxel (PTX), the Fe_3O_4@Cs-PEG-PTX-FA nanoparticles showed an increased size, ranging between 100-120 nm as shown Figure 7(b).

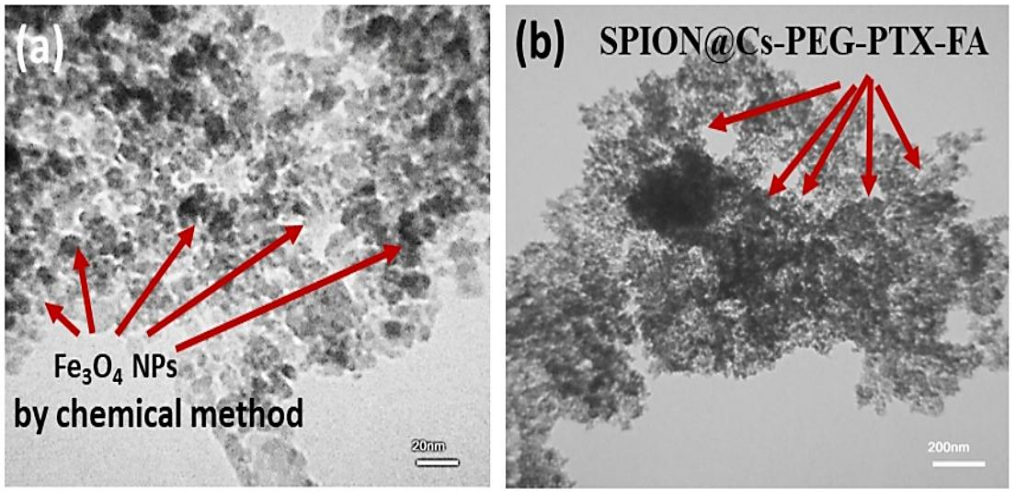

Figure 7: TEM of Fe_3O_4 NP prepared by chemical method (a) before coating and Fe_3O_4@Cs-PEG-PTX-FA (b)

The particle size data obtained from TEM is consistent with the findings from Field Emission Scanning Microscopy (FESM), confirming the accuracy of the particle size estimation for both Fe_3O_4 and Fe_3O_4@Cs-PEG-PTX-FA nanoparticles. The strong agreement between the two characterization techniques reinforces the reliability of the synthesis and coating methods used, ensuring uniform particle sizes crucial for maintaining the desired physical, chemical, and magnetic properties. This consistency between FESM and TEM results is pivotal for biomedical applications, particularly in targeted drug delivery systems, where size uniformity directly influences efficacy and precision.

It is generally known that the shape, size of particles, and dimensions displayed direct impacts on the magnetic characteristics of Fe_3O_4 NPs. Figure 8 displays the result of VSM. During the magnetic measurement, at ambient temperature, the application of a magnetic field had a range of -1 to 1 T. The superparamagnetic characteristics of the Fe_3O_4@Cs-PTX-PEG-FA nanosystem with a saturation magnetization value of 59.6 emu/mg were also shown by the curves. Fe_3O_4 has a saturation magnetization value (Ms) of 59.6 emu/gram. This investigation demonstrated that Fe_3O_4@Cs-PTX-PEG-FA NPs are suitable nanocarriers due to their quick reaction to an external magnetic field and their stable structure in solution. Furthermore, the Hc value of near 0 [32-34] and the crystallite size of less than 50 nm Fe_3O_4 shown by the VSM result indicate that this material exhibits superparamagnetic behavior at ambient temperature. Based on the Ms value, the current findings exhibited that Fe_3O_4 has a high potential for use in biological applications, particularly nanocarriers. According to Brusentsov et al. [35], Fe_3O_4 can be used in biological applications if its Ms value is between 5 and 25 emu/g.

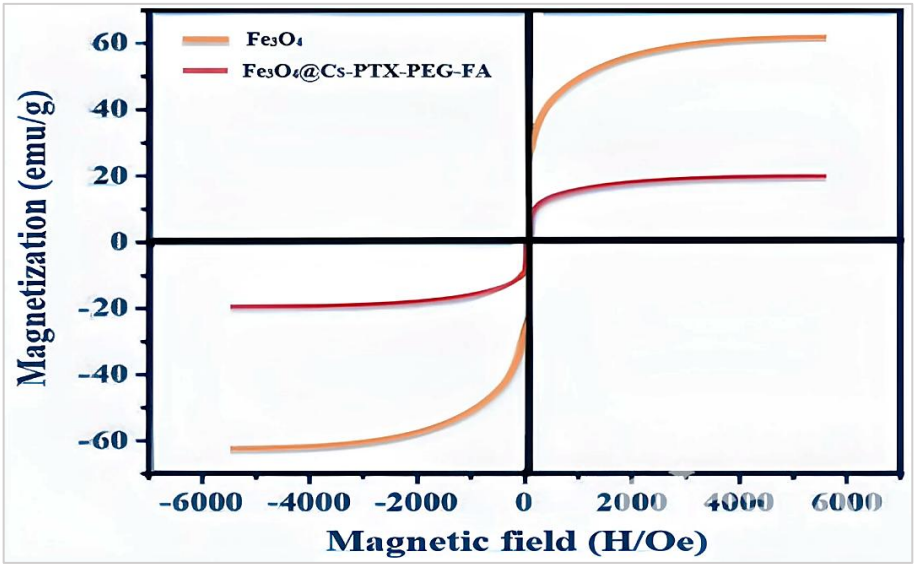

Figure 8: Magnetization curve of Fe_3O_4 before and after coating with polymers

4. Conclusion

Co-precipitation was used to create Fe_3O_4 NPs using iron salts as the starting material, further encapsulated to form Fe_3O_4@Cs-PEG-PTX-FA nanocarriers. Where the stirring rate and temperature have crucial impacts on the size and quality of crystallite Fe_3O_4, XRD confirmed the crystalline structure and purity of the synthesized materials with no detectable secondary phases. It is evident from the magnetic characterization that Fe_3O_4 was used in this study. Notably, the nanocarriers exhibit superparamagnetic behavior at ambient temperature. This nature ensures stability and controlled drug release at the target site, reducing off-target effects. The functional coatings enhance circulation time and targeting efficiency, addressing critical challenges in cancer therapy. Encapsulation efficiency of 82.4% and drug-loading content of 14.4% were achieved, indicating effective incorporation of PTX into the nanocarriers. These results underscore the potential of these nanocarriers to deliver therapeutic agents efficiently. In addition to size uniformity, biocompatibility, and responsiveness to external magnetic fields, these properties make them promising candidates for cancer treatment, particularly in targeting fibrosarcoma cells.

Acknowledgments

The authors extend their sincere gratitude for the technical support offered by the Applied Sciences Department at the University of Technology, Baghdad, Iraq, and the Department of Electrical, Engineering, and Built Environment at Universiti Kebangsaan Malaysia (UKM).

Author contributions

Conceptualization, **A. Haider**, **S. Al-Musawi**, **R. Al-Obaidy**, **A. Haleem**, **M. Al-Hindawi**, and **B. Taha**; data curation, **A. Haider**, and **B. Taha**; formal analysis, **A. Haider**, and **S. Al-Musawi**; investigation, **A. Haider**, and **S. Al-Musawi**; methodology, **A. Haider**, **M. AL-Hindawi**, and **S. Al-Musawi**; project administration, **A. Haider**, and **S. Al-Musawi**, resources, **R. Al-Obaidy**, and **A. Haleem**; supervision, **A. Haider**, and **S. Al-Musawi**; validation, **A. Haider**, **R. Al-Obaidy**, and **A. Haleem**; visualization, **B. Taha**, and **S. Al-Musawi**; writing—original draft preparation, **A. Haider**, **A. Haleem**, and **S. Al-Musawi**; writing—review and editing, **B. Taha**, and **S. Al-Musawi**. All authors have read and agreed to the published version of the manuscript.

Funding

This research received no specific grant from any funding agency in the public, commercial, or not-for-profit sectors.

Data availability statement

The data that support the findings of this study are available on request from the corresponding author.

Conflicts of interest

The authors declare that there is no conflict of interest.

References

[1] N. Bock, A. Riminucci, C. Dionigi, A. Russo, A. Tampieri, E. Landi, V.A. Goranov, M. Marcacci, V. Dediu, A novel route in bone tissue engineering: Magnetic biomimetic scaffolds, J. Acta Biomater., 6 (2010) 786–796. https://doi.org/10.1016/j.actbio.2009.09.017

[2] Y. Chen, G. Lian, C. Liao, W. Wang, L. Zeng, C. Qian, K. Huang, X. Shuai, Characterization of polyethylene glycol-grafted polyethyleneimine and superparamagnetic iron oxide nanoparticles (PEG-g-PEI-SPION) as an MRI-visible vector for siRNA delivery in gastric cancer in vitro and in vivo, Am. J. Gastroenterol., 48 (2013) 809–821. https://doi.org/10.1007/s00535-012-0713-x

[3] S. I. Jenkins, H. H. P. Yiu, M. J. Rosseinsky, D. M. Chari, Magnetic nanoparticles for oligodendrocyte precursor cell transplantation therapies: progress and challenges, Mol. Cell. Ther., 2 (2014) 23. https://doi.org/10.1186/2052-8426-2-23

[4] R. Al-Obaidy, A. J. Haider, S. Al-Musawi, N. Arsad, Targeted delivery of paclitaxel drug using polymer-coated magnetic nanoparticles for fibrosarcoma therapy: in vitro and in vivo studies, Sci. Rep., 13 (2023) 3180. https://doi.org/10.1038/s41598-023-30221-x

[5] P. Varallyay, G. Nesbit, L. L. Muldoon, R. R. Nixon, J. Delashaw, J. I. Cohen, A. Petrillo, D. Rink, E. A. Neuwelt, Comparison of two superparamagnetic viral-sized iron oxide particles ferumoxides and ferumoxtran-10 with a gadolinium chelate in imaging intracranial tumors, AJNR Am. J. Neuroradiol., 23 (2002) 510–519.

[6] C. Li , T. Chen , I. Ocsoy , G. Zhu , E. Yasun , M. You , C. Wu , J. Zheng , E. Song , C. Z. Huang ,W. Tan, Gold-Coated Fe_3O_4 Nanoroses with Five Unique Functions for Cancer Cell Targeting, Imaging, and Therapy, Adv. Funct. Mater., 24 (2014) 1772-1780. https://doi.org/10.1002/adfm.201301659

[7] M. A. Al-Kinani, A. Haider, S. Al-Musawi, Study the effect of laser wavelength on polymeric metallic nanocarrier synthesis for curcumin delivery in prostate cancer therapy: in vitro study, J. Appl. Sci. Nanotechnol., 1 (2021) 43-50. http://dx.doi.org/10.53293/jasn.2021.11023

[8] C. Wilhelm, F. Gazeau, Universal cell labelling with anionic magnetic nanoparticles, Biomaterials. 29 (2008) 3161–3174. https://doi.org/10.1016/j.biomaterials.2008.04.016

[9] M. Johannsen, U. Gneveckow, L. Eckelt, A. Feussner, N. Waldo Fner, R. Scholz, S. Deger, P. Wust, S.A. Loening, A. Jordan, Clinical hyperthermia of prostate cancer using magnetic nanoparticles: Presentation of a new interstitial technique, Int. J. Hyperthermia., 21(2005) 637–647. https://doi.org/10.1080/02656730500158360

[10] A. J. Haider, A. D. Thamir, D. S. Ahmed, M. R. Mohammad, Deposition of silver nanoparticles on multiwalled carbon nanotubes by chemical reduction process and their antimicrobial effects, AIP Conf. Proc., 1758, 2016, 030003. http://dx.doi.org/10.1063/1.4959399

[11] A. A. Yousif, N. F. Habubi, A. A. Haidar, Nanostructure zinc oxide with cobalt dopant by PLD for gas sensor applications, J. Nano Electron. Phys., 4 (2012) 1-6.

[12] P. Simamora, C. S. Saragih, D. P. Hasibuan, and J. Rajagukguk, Synthesis of nanoparticles Fe_3O_4 /PEG/PPy-based on natural iron sand, Mater. Today Proc., 5 (2018) 14970–14974. http://dx.doi.org/10.1016/j.matpr.2018.04.040

[13] M. Anbarasu, M. Anandan, E. Chinnasamy, V. Gopinath, K. Balamurugan, Synthesis and characterization of polyethylene glycol (PEG) coated Fe_3O_4 nanoparticles by chemical co-precipitation method for biomedical applications, Spectrochim. Acta, Part A., 135,(2015) 536–539. https://doi.org/10.1016/j.saa.2014.07.059

[14] A. Radoń, D. Łukowiec, M. Kremzer, J. Mikuła, P. Włodarczyk, Electrical Conduction Mechanism and Dielectric Properties of Spherical Shaped Fe_3O_4 Nanoparticles Synthesized by Co-Precipitation Method, Materials, 11 (2018) 1-12. https://doi.org/10.3390/ma11050735

[15] Y. S. Kang, S. Risbud, J. F. Rabolt, P. Stroeve, Synthesis and characterization of nanometer-size Fe_3O_4 and γ-Fe_2O_3 particles, Chem. Mater., 8 (1996) 2209–2211. https://doi.org/10.1021/cm960157j

[16] M. M. Nosan., Magnetic properties of nanoparticles prepared from α-Fe target by laser ablation in liquids, Prog. Electromagn. Res. Symp., 2017, 109-113. https://doi.org/10.1109/PIERS-FALL.2017.8293120

[17] M. d. N. Islam, L.V. Phong, J. R. Jeong, C. G. Kim, A facile route to sonochemical synthesis of magnetic iron oxide (Fe3O4) nanoparticles, J. Thin Solid Films. 519 (2011) 8277–8279. https://doi.org/10.1016/j.tsf.2011.03.108

[18] J. Y. Choi, R. K. Thapa, C. S. Yong, and J. O. Kim, Nanoparticle-based combination drug delivery systems for synergistic cancer treatment, J. Pharm. Investig., 46 (2016) 325–339. https://doi.org/10.1007/s40005-016-0252-1

[19] A. Sood, V. Arora, J. Shah, R. K. Kotnala, and T. K. Jain, Multifunctional gold-coated iron oxide core-shell nanoparticles stabilized using thiolated sodium alginate for biomedical applications, Mater. Sci. Eng. C, 80 (2017) 274–281. https://doi.org/10.1016/j.msec.2017.05.079

[20] M. Al-Kinani, A. Haider, and S. Al-Musawi, Study the Effect of Laser Wavelength on Polymeric Metallic Nanocarrier Synthesis for Curcumin Delivery in Prostate Cancer Therapy: In Vitro Study, J. Appl. Sci. Nanotechnol., 1 (2021) 43–50. https://doi.org/10.53293/jasn.2021.11023

[21] S. Al-musawi, Folated-nanocarrier for curcumin drug delivery in breast cancer therapy, Eng. Technol. J., 33 (2015) 1643-1654. https://doi.org/10.30684/etj.2015.117372

[22] A. Ahmad, M. M. Ansari, A. Kumar, A. Vyawahare, R. K. Mishra, G. Jayamurugan, S. S. Raza, R. Khan, Comparative acute intravenous toxicity study of triple polymer-layered magnetic nanoparticles with bare magnetic nanoparticles in Swiss albino mice, Nanotoxicology, 14 (2020) 1362-1380. https://doi.org/10.1080/17435390.2020.1829144

[23] F. S. Abdulwahid, A. J. Haider, S. Al-Musawi, Iron Oxide Nanoparticles (IONPs): Synthesis, Surface Functionalization, and Targeting Drug Delivery Strategies: Mini-Review, Nano, 17 (2022) 1-15. https://doi.org/10.1142/S1793292022300079

[24] A. A. Atiyah,A. J. Haider, R. M. Dhahi, Cytotoxicity properties of functionalized carbon nanotubes on pathogenic bacteria. IET nanobiotechnology, 13 (2019) 597-601. http://dx.doi.org/10.1049/iet-nbt.2018.5394

[25] Devra V. Biological Synthesis of Metal Nanoparticles: A Review, Academia Letters, 2022.

[26] M. J. Rivera-Chaverra, E. Restrepo-Parra, C. D. Acosta-Medina, A. Mello, R. Ospina, Synthesis of oxide iron nanoparticles using laser ablation for possible hyperthermia applications, Nanomaterials, 10 (2020) 1-12. https://doi.org/10.3390/nano10112099

[27] A. J. Haider, M. A. Al-Kinani, S. Al-Musawi, Preparation and Characterization of Gold Coated Super Paramagnetic Iron Nanoparticle Using Pulsed Laser Ablation in Liquid Method, Key Eng. Mater., 886 (2021) 77-85. https://doi.org/10.4028/www.scientific.net/KEM.886.77

[28] D. Q. Hoang, T. V. Tran, N. Q. Tran, C. K. Nguyen, T. H. Nguyen, M. D. Truong, D. H. Nguyen, Functionalization of Fe_3O_4 nanoparticles with biodegradable chitosan-grafted-mPEG for paclitaxel delivery, Green Process. Synth., 5 (2016) 459-466. http://dx.doi.org/10.1515/gps-2016-0093

[29] S. Sunaryono, A. Taufiq, M. Mashuri, S. Pratapa, M. Zainuri, T. Triwikantoro, D. Darminto Various Magnetic Properties of Magnetite Nanoparticles Synthesized from Iron-sands by Coprecipitation Method at Room Temperature, Mater. Sci. Forum, 827 (2015) 229-234. https://doi.org/10.4028/www.scientific.net/MSF.827.213

[30] G. Baldia, D. Bonacchia, C. Innocentib, G. Lorenzia, C. Sangregori, Cobalt ferrite nanoparticles: The control of the particle size and surface state and their effects on magnetic properties, J. Magn. Magn. Mater., 311 (2007) 10– 16. http://dx.doi.org/10.1016/j.jmmm.2006.11.157

[31] F. S. Abdulwahid, A. J. Haider, S. Al-Musawi, Folate decorated dextran-coated magnetic nanoparticles for targeted delivery of ellipticine in cervical cancer cells, Adv. Nat. Sci.: Nanosci. Nanotechnol., 14 (2023) 1-10. http://dx.doi.org/10.1088/2043-6262/aca606

[32] Q. Zhang, R. Chen, J. Gong, M. Yuan, L. Chen, Single-crystalline Fe_3O_4 nanosheets: Facile sonochemical synthesis, evaluation and magnetic properties, J. Alloys Compd., 577 (2013) 528–532. https://doi.org/10.1016/j.jallcom.2013.06.176

[33] A. Taufiq, S. Sunaryono, E. G. R. Putra, A. Okazawa, I. Watanabe, N. Kojima, S. Pratapa ,D. Darminto, Nanoscale Clustering and Magnetic Properties of MnxFe3−xO4 Particles Prepared from Natural Magnetite, J. Supercond Nov Magn., 28 (2015) 2855– 2863. http://dx.doi.org/10.1007/s10948-015-3111-9

[34] M. A. Al-Kinani, A. J. Haider, S. Al-Musawi, High Uniformity Distribution of Fe@Au Preparation by a Micro-Emulsion Method. IOP Conf. Ser.: Mater. Sci. Eng., 987, 2020, 012013. http://dx.doi.org/10.1088/1757-899X/987/1/012013

[35] N. A. Brusentsov, V.V. Gogosov, T.N. Brusentsova, A.V. Sergeev, N.Y. Jurchenko, A.A. Kuznetsov, O. A. Kuznetsov, L.I. Shumakov , Evaluation of ferromagnetic fluids and suspensions for the site-specific radio frequency-induced hyperthermia of MX11 sarcoma cells in vitro, J. Magn. Magn. Mater., 225 (2011) 113-117. https://doi.org/10.1016/S0304-8853(00)01238-5